Article:
Harrison, J. R., Akers, R. J., Allan, S. Y. et al. (115 more authors) (2019) Overview of new MAST physics in anticipation of first results from MAST Upgrade. Nuclear Fusion. 112011. ISSN 1741-4326

https://doi.org/10.1088/1741-4326/ab121c

Overview of new MAST Physics in Anticipation of First Results from MAST Upgrade

JR Harrison[1], RJ Akers[1], SY Allan[1], JS Allcock[1,2], JO Allen[3], L Appel[1], M Barnes[1,4,5], N Ben Ayed[1], W Boeglin[6], C Bowman[3], J Bradley[7], P Browning[8], P Bryant[7], M Carr[1], M Cecconello[9], CD Challis[1], S Chapman[10], IT Chapman[1], GJ Colyer[4,11], S Conroy[9], NJ Conway[1], M Cox[1], G Cunningham[1], RO Dendy[1,10], W Dorland[4,19], BD Dudson[3], L Easy[1,3], SD Elmore[1], T Farley[1,7], X Feng[2], AR Field[1], A Fil[3], GM Fishpool[1], M Fitzgerald[1], K Flesch[12], MFJ Fox[1,4,13], H Frerichs[12], S Gadgil[10], D Gahle[1,14], L Garzotti[1], Y-C Ghim[1,4,20], S Gibson[1,2], KJ Gibson[3], S Hall[1], C Ham[1], N Heiberg[1], SS Henderson[1], E Highcock[4,21], B Hnat[10], J Howard[15], J Huang[22], SWA Irvine[10], AS Jacobsen[23], O Jones[1,2], I Katramados[1], D Keeling[1], A Kirk[1], I Klimek[9], L Kogan[1], J Leland[1,7], B Lloyd[1], J Lovell[16], B Madsen[17], O Marshall[3], R Martin[1], G McArdle[1], K McClements[1], B McMillan[10], A Meakins[1], HF Meyer[1], F Militello[1], J Milnes[1], S. Mordijck[24], AW Morris[1], D Moulton[1], D Muir[1], K Mukhi[1,8], S Murphy-Sugrue[1,7], O. Myatra[3], G Naylor[1], P Naylor[3], SL Newton[1], T O'Gorman[1], J Omotani[1], MG O'Mullane[14], S Orchard[1,3], SJP Pamela[1], L Pangione[1], F Parra[1,4], RV Perez[6], L Piron[1], M Price[1], ML Reinke[16], F Riva[1], CM Roach[1], D Robb[25], D Ryan[1], S Saarelma[1], M Salewski[17], S Scannell[1], AA Schekochihin[4,13], O Schmitz[12], S Sharapov[1], R Sharples[2], SA Silburn[1], SF Smith[1,3], A Sperduti[9], R Stephen[1], NT Thomas-Davies[1], AJ Thornton[1], M Turnyanskiy[1], M Valovič[1], F Van Wyk[1,4,18], RGL Vann[3], NR Walkden[1], I Waters[12], HR Wilson[1,3] and the MAST-U Team and the EUROfusion MST1 team[*]

[1] CCFE, Culham Science Centre, Abingdon, Oxon, OX14 3DB, United Kingdom
[2] Centre for Advanced Instrumentation, Durham University, South Road, Durham, DH1 3LE, United Kingdom
[3] York Plasma Institute, Department of Physics, University of York, Heslington, York YO10 5DD, United Kingdom
[4] Rudolf Peierls Centre for Theoretical Physics, University of Oxford, OX1 3PU, United Kingdom
[5] Plasma Science and Fusion Center, 167 Albany Street, Cambridge, MA 02139, United States of America
[6] Department of Physics, Florida International University, 11200 SW, Miami, FL 33199, United States of America
[7] Department of Electrical Engineering and Electronics, University of Liverpool, Brownlow Hill, Liverpool L69 3GJ, United Kingdom
[8] School of Physics and Astronomy, University of Manchester, Oxford Road, Manchester M13 9PL, United Kingdom
[9] Department of Physics and Astronomy, Uppsala University, SE-751 05 Uppsala, Sweden
[10] Centre for Fusion, Space and Astrophysics, Department of Physics, University of Warwick, Coventry, CV4 7AL, United Kingdom
[11] Engineering, Mathematics and Physical Sciences, University of Exeter, EX4 4QF, United Kingdom
[12] University of Wisconsin-Madison, Madison, Wisconsin, United States of America
[13] Merton College, Oxford, OX1 4JD, United Kingdom
[14] Department of Physics SUPA, University of Strathclyde, Glasgow, G4 ONG, United Kingdom

[*] See the author list of "H. Meyer et al 2017 Nucl. Fusion 57 102014"

[15] Plasma Research Laboratory, Australian National University, Canberra, ACT 0200, Australia
[16] Oak Ridge National Laboratory, Oak Ridge, TN 37831, United States of America
[17] Department of Physics, Technical University of Denmark, Kgs. Lyngby, Denmark
[18] STFC Daresbury Laboratory, Daresbury, Cheshire, WA4 4AD, United Kingdom
[19] Department of Physics, University of Maryland, College Park, MD 20742-4111, United States of America
[20] Department of Nuclear and Quantum Engineering, KAIST, Daejeon, 34141, Republic of Korea
[21] Chalmers University of Technology, Department of Physics, Göteborg SE-412 96, Sweden
[22] Institute of Plasma Physics, Chinese Academy of Sciences, P.O. 1126, 230031 Hefei, Anhui, China
[23] Max-Planck-Institut für Plasmaphysik, Garching, Germany
[24] Dept. of Computer Science, College of William & Mary, Williamsburg, VA, United States of America
[25] Department of Physics and Astronomy, University of Glasgow, Glasgow G12 8QQ, United Kingdom

Abstract

The Mega Amp Spherical Tokamak (MAST) was a low aspect ratio device (R/a = 0.85/0.65 ~ 1.3) with similar poloidal cross-section to other medium-size tokamaks. The physics programme concentrates on addressing key physics issues for the operation of ITER, design of DEMO and future spherical tokamaks by utilising high resolution diagnostic measurements closely coupled with theory and modelling to significantly advance our understanding. An empirical scaling of the energy confinement time that favours higher power, lower collisionality devices is consistent with gyrokinetic modelling of electron scale turbulence. Measurements of ion scale turbulence with beam emission spectroscopy and gyrokinetic modelling in up-down symmetric plasmas find that the symmetry of the turbulence is broken by flow shear. Near the non-linear stability threshold, flow shear tilts the density fluctuation correlation function and skews the fluctuation amplitude distribution. Results from fast particle physics studies include the observation that sawteeth are found to redistribute passing and trapped fast particles injected from neutral beam injectors in equal measure, suggesting that resonances between the m=1 perturbation and the fast ion orbits may be playing a dominant role in the fast ion transport. Measured D-D fusion products from a neutron camera and a charged fusion product detector are 40% lower than predictions from TRANSP/NUBEAM, highlighting possible deficiencies in the guiding centre approximation. Modelling of fast ion losses in the presence of resonant magnetic perturbations (RMPs) can reproduce trends observed in experiments when the plasma response and charge-exchange losses are accounted for. Measurements with a neutral particle analyser during merging-compression start-up indicate the acceleration of ions and electrons. Transport at the plasma edge has been improved through reciprocating probe measurements that have characterised a geodesic acoustic mode at the edge of an ohmic L-mode plasma and particle-in-cell modelling has improved the interpretation of plasma potential estimates from ball-pen probes. The application of RMPs leads to a reduction in particle confinement in L-mode and H-mode and an increase in the core ionization source. The ejection of secondary filaments following type-I ELMs correlates with interactions with surfaces near the X-point. Simulations of the interaction between pairs of filaments in the scrape-off layer suggest this results in modest changes to their velocity, and in most cases can be treated as moving independently. A stochastic model of scrape-off layer profile formation based on the superposition of non-interacting filaments is in good agreement with measured time-average profiles. Transport in the divertor has been improved through fast camera imaging, indicating the presence of a quiescent region devoid of filament near the X-point, extending from the separatrix to $\psi_n \sim 1.02$. Simulations of turbulent transport in the

divertor show that the angle between the divertor leg on the curvature vector strongly influences transport into the private flux region via the interchange mechanism. Coherence imaging measurements show counter-streaming flows of impurities due to gas puffing increasing the pressure on field lines where the gas is ionised. MAST Upgrade is based on the original MAST device, with substantially improved capabilities to operate with a Super-X divertor to test extended divertor leg concepts. SOLPS-ITER modelling predicts the detachment threshold will be reduced by more than a factor of 2, in terms of upstream density, in the Super-X compared with a conventional configuration and that the radiation front movement is passively stabilised before it reaches the X-point. 1D fluid modelling reveals the key role of momentum and power loss mechanisms in governing detachment onset and evolution. Analytic modelling indicates that long legs placed at large major radius, or equivalently low $|\mathbf{B}|$ at the target compared with the X-point are more amenable to external control. With MAST Upgrade experiments expected in 2019, a thorough characterisation of the sources of the intrinsic error field has been carried out and a mitigation strategy developed.

1. Introduction

The Mega Amp Spherical Tokamak (MAST) was a low aspect ratio device (R/a = 0.85/0.65 ~1.3, $I_p \leq$ 1.3MA, $B_\varphi(R_0) \leq 0.52$T) with a similar cross-section to other medium-size tokamaks (e.g. ASDEX Upgrade [1]) and, together with NSTX-U [2] was one of the two largest spherical tokamaks. Advances in our understanding of key physics issues concerning the operation of ITER [3] and the design of DEMO [4][5] have been made by utilising high resolution diagnostics together with sophisticated numerical modelling. MAST operations finished in October 2013 to enable the construction of MAST Upgrade. Since then, substantial data analysis and modelling activities have been performed to validate models to improve our capability to extrapolate to future devices, in particular MAST Upgrade [6][7].

The construction of MAST Upgrade has recently been completed and features substantially improved capabilities over the previous MAST device. These include 17 new poloidal field coils (14 of which are within the vacuum vessel), new closed, up-down symmetric divertors with Super-X capability fitted with cryopumps, 50% higher toroidal field (from 0.585T to 0.92T at R=0.7m) and a new solenoid will nearly double the inductive flux from 0.9Vs to 1.7Vs, allowing for the maximum plasma current and pulse length to be 2MA and 5s respectively (from 1.35MA and 0.7s), although not concurrently. Operation at maximum current and toroidal field will enable pulses up to ~2s flat-top duration and a maximum plasma current of 1MA will be sustained for up to 5s. A combination of on and off-axis neutral beam heating and current drive to tailor the fast ion distribution and q profile to avoid MHD instabilities. The planned physics programme emphasises utilisation of its unique divertor and core capabilities to address key issues for the success of ITER operations and the design of future devices [7], including exploring reactor-relevant alternative divertor configurations, adding to the knowledge base for ITER and to explore the performance of spherical tokamaks at higher magnetic field, shaping and auxiliary heating.

This paper describes results from MAST, starting from the plasma core, data and gyrokinetic modelling of ion scale turbulence and simulations of electron scale turbulence are discussed in section 2. In section 3, the impact of sawteeth and Resonant Magnetic Perturbations (RMPs) on fast ion confinement, characterisation of a neutron deficit and evidence for the acceleration of electrons and ions during merging-compression start-up on MAST are discussed. In section 4, new insights into transport at the edge of the confined plasma using a reciprocating probe are presented, including measurements of a Geodesic Acoustic Mode, the impact of RMPs on particle confinement, measurements of secondary ELM filaments in MAST and initial modelling of ELMs in MAST-U with JOREK are presented. In section 5, measurements and modelling of transport in the divertor and scrape-off layer are presented, together with modelling of detachment and the influence of the divertor geometry on its access and evolution. An overview of the preparations for initial operations of MAST Upgrade are presented in

section 6, with details of a package of further enhancements to address key gaps in our understanding of plasma exhaust approaching reactor relevant conditions.

2. Core Transport & Confinement

Spherical tokamaks such as MAST are an excellent environment for studying core transport in very challenging conditions with high β, strongly driven toroidal flow (and flow shear) and fast ion pressure. Previous experiments on MAST and NSTX found that the energy confinement time varied according to the scaling $B\tau_E \propto \nu_*^{-0.82\pm0.1}$ [8][9], where B is the magnetic field, τ_E is the energy confinement time and ν_* is collisionality, which is favourable for higher power devices with closed divertors that can reach lower collisionality such as MAST Upgrade. We note that this trend is consistent with recent electrostatic simulations of Electron Temperature Gradient (ETG) scale turbulence at mid-radius in a MAST H-mode plasma[1] using the gyrokinetic flux-tube code GS2 [10] with adiabatic ions. On running ETG simulations at low collisionality for sufficiently long durations (~$0.01\tau_E$) [13], it is found that the dominant radially elongated streamer-like structures of an early "quasi-saturated" state become suppressed by slowly growing zonal modes that reduce turbulence (and its associated transport) to reach a saturated state that is dominated by "vortex streets", as shown in Figure 1. The fully saturated electron heat flux is found to scale linearly with collisionality due to the damping of zonal modes by collisions, which provides a candidate mechanism to explain the favourable ST scaling of energy confinement with collisionality. Other candidate mechanisms have previously been proposed based on the collision dependence of microtearing mode linear growth rates [15] and on the collision dependence of dissipative trapped electron mode turbulence [16].

Transport due to ion scale turbulence is normally strongly suppressed by flow shear which alters the characteristics of the remaining structures generated by the turbulence. Sophisticated analysis techniques have been applied to Beam Emission Spectroscopy (BES) data, taking account of the finite spatial resolution [17] to extract spatial and temporal correlation parameters of density fluctuations in neutral beam heated plasmas. In up-down symmetric double null plasmas, toroidal flow shear breaks the symmetry of the turbulence [18]. Sheared equilibrium flow shears turbulent eddies, resulting in a tilt of the spatial correlation function, which increases with flow shear, as shown in Figure 2. Close to the non-linear threshold, the shear also skews the amplitude distribution of the density fluctuations. These observations are not inconsistent with results of non-linear gyro-kinetic simulations of ion-scale turbulence for a MAST equilibrium, close to threshold normalised temperature gradient required for the excitation of sub-critical turbulence, in which the turbulence is found to be dominated by a few, isolated,

[1] Gyrokinetic simulations have previously suggested that ETG turbulence can give rise to experimentally relevant levels of electron heat transport at mid-radius in MAST H-mode plasmas [10][11], and that the turbulence at ion scales is often suppressed by flow shear [12]. In [13], an analysis at mid-radius in the MAST H-mode discharge #8500 with 2MW of Neutral Beam Injection heating. Its data are available in the International Multi-Tokamak Profile Database [14].

long-lived structures [19]. The simulations suggest that further from the threshold, the symmetry is effectively restored, reducing both the tilt of the correlation function and skewness of the distribution.

3. Fast Particle Physics

In future devices where a significant proportion of the plasma heating comes from alpha-particles generated by fusion reactions, confinement of energetic particles in the presence of MHD instabilities that cause the redistribution, and sometimes loss, of energetic particles, is a significant issue. Sawteeth invariably result in the redistribution of fast particles, but a high fast particle population inside the q=1 surface extends the sawtooth period, resulting in a larger crash, which can lead to the triggering of instabilities such as Neoclassical Tearing Modes (NTMs) that significantly degrade plasma confinement [20]. Studies of the effects of sawteeth on fast ion confinement in MAST [21], based principally on neutron camera data, suggest that passing and trapped fast particles are redistributed in approximately equal measure. The amplitude of the fast ion redistribution, inferred from neutron camera and Fast Ion D-alpha (FIDA) measurements, is consistent with TRANSP [22] / NUBEAM [23] simulations. Three separate sawtooth models are all compatible with the measured impact of sawteeth on neutron emission profiles: the Kadomtsev model [24] which assumes full reconnection inside the q=1 surface, both including and excluding ergodisation; and the Porcelli model [25], in which incomplete reconnection is assumed to occur. No evidence has been found of an energy threshold for redistribution of passing or trapped particles due to sawteeth, suggesting that resonances between the m=1 sawtooth perturbation and the fast ion orbit (both the poloidal bounce and toroidal precession) frequencies may be playing a dominant role in the fast ion transport. Further insights into the effects of sawteeth on fast ion confinement have been derived from a novel tomographic reconstruction technique applied to FIDA data to reconstruct the fast particle distributions, in pitch and energy space, before and after a sawtooth [26]. The inverted data, shown in Figure 3, indicate a 42% reduction across the fast ion density profile with a modest change in its shape, comparable to but slightly lower than a 46% reduction predicted by TRANSP/FIDASIM simulations.

Fusion reactions on MAST occur primarily due to the interaction between energetic neutral deuterons generated by a Neutral Beam Injector (NBI) and thermal deuterium ions in the plasma, contributing ~90%, and the remainder are mainly due to interactions between energetic particles delivered by the NBIs making up most of the remaining ~10%. The fusion reaction rate of this process is well known, so any discrepancy between calculated and measured fluxes of fusion products is expected to be due to errors in the assumed deposition profile of the neutral beam(s), or processes such as fuel dilution or the transport of fast ions [27]. Recent analysis of fusion product fluxes measured independently with a neutron camera [28] and charged fusion product detector [29] indicates that these are approximately 40% lower than those predicted by the TRANSP/NUBEAM codes [30], independent of the plasma

scenario. An anomalous fast ion diffusivity is sometimes required to obtain a good match between TRANSP/NUBEAM and the neutron camera measurements, ranging from zero in quiescent scenarios to 3 m^2s^{-1} when MHD instabilities are present. The discrepancy cannot be explained by uncertainties in the measured plasma profiles of the main ions or impurities, or the injected neutral beam power. A possible explanation is that the guiding centre approximation used in NUBEAM leads to an over-estimate of the neutron emissivity. It is expected that the guiding centre approximation is inaccurate on spherical tokamaks such as MAST due to the low confining magnetic field, which means that the Larmor radii of fast ions are a significant fraction of the length scales of plasma profiles. This inaccuracy appears to persist even when using a Finite Larmor Radius correction algorithm available in NUBEAM [31]. This will motivate future studies with full orbit following codes.

In future large, high power fusion experiments such as ITER, it is anticipated that techniques such as the application of Resonant Magnetic Perturbations will be required to mitigate or suppress Edge Localised Modes (ELMs) that would otherwise pose a risk to the integrity of plasma-facing surfaces on the first wall and divertor [32]. The application of RMPs with a toroidal mode number of 3 to low current (I_p = 400kA) H-mode plasmas results in a degradation of fast ion confinement, indicated by a factor ~2 reduction in the neutron rate measured by a fission chamber. Simulations of fast ion losses caused by RMPs were carried out using a non-steady-state orbit-following Monte-Carlo code (NSS OFMC), showing that both the plasma response to the RMPs and charge-exchange reactions with background neutrals must be taken into account [31]. In experiments, the application of RMPs with higher toroidal mode number or operation at higher plasma current is found to considerably diminish the reduction in the measured neutron rate.

Studies of neutral particle analyser (NPA) and microwave data have revealed that magnetic reconnection during merging-compression plasma start-up in MAST resulted in the acceleration of both ions and electrons [33]. While merging-compression will not be used as a start-up method in MAST Upgrade, it is intended that particle acceleration due to other types of reconnection event will be studied using new fast ion diagnostics, including a scintillator-based fast ion loss detector [34] and a solid state Neutral Particle Analyser.

4. Edge, Pedestal & ELMs

Understanding the transport mechanisms prevailing at the plasma edge is essential to understand and predict global confinement and L-H transitions. Detailed measurements of electrostatic potential fluctuations have yielded new observations of mode activity that has been found on several devices to regulate the transport in this region (e.g. on DIII-D [35], AUG [36], HL-2A [37] and others). Measurements from an ohmic L-mode plasma indicate the presence of a Geodesic Acoustic Mode (GAM) 2cm inside the separatrix, with a frequency of ~10kHz, maximum radial mode number $k_r\rho_p$ ~ -

0.15 and radial phase velocity of 1km/s [38]. Further studies are on-going to ascertain the impact of the GAM on transport in this region.

Ball-pen probes mounted into reciprocating probe heads [39] [40], have been used to obtain an estimate of the radial profile of plasma potential and T_e. They consist of a Langmuir probe recessed from the surface of the reciprocating probe shadowed from the majority of plasma ions in order to equalise the fluxes of ions and electrons to the probe such that the probe floats at the plasma potential. Analysis of the data collected has been complicated by an incomplete understanding of the mechanisms that transport ions and electrons to the probe surface. These transport mechanisms have been elucidated using particle-in-cell modelling, showing ions reach the recessed Langmuir probe via a combination of their Larmor orbits and ExB drifts due to electrons polarising the material leading to the probe [41].

The application of RMPs to L-mode and H-mode plasmas has been shown to degrade particle confinement, often referred to as a "density pump-out" on MAST [42] DIII-D [43] JET [44] and other devices. The effects of RMPs on particle confinement have been quantified by applying a global particle balance model [45] constrained by the measured fuelling rates from gas valves and neutral beam injection, and particle sources in the main chamber from the intensity of D_α emission. The particle confinement time is found to reduce by ~20% in L-mode and ~30% in H-mode between ELMs relative to before the RMP was applied, where perturbations with toroidal mode numbers n=3 or 4 were applied respectively, as shown in Figure 4. In L-mode and H-mode during inter-ELM periods, the application of RMPs leads to increased D_α emission at the outer mid-plane, suggesting an increase in neutral fuelling that partially compensates for the reduction in particle confinement on the core density profiles [46].

The characteristics of unmitigated ELMs have been studied using fast imaging data, showing that in certain magnetic configurations, following the ejection of type-I ELMs, secondary filaments have been observed up to 1ms following the ELM, concurrent with an increase in the width of the SOL. The appearance of secondary filaments correlates with plasma interaction with poloidal field coils near the X-point. This will be the subject of further study in MAST-U using the baffling structures at the entrance to the closed divertors.

Initial simulations of the propagation of large type-I ELMs through a Super-X divertor configuration in MAST-U have been carried out using the JOREK code [47] with the addition of a simplified fluid model describing the transport of neutrals. The simulations show the ELM burning through the cold (T_e < 5eV), dense plasma in the divertor, as illustrated in Figure 5. These and future simulations will be used to guide experiments exploring whether closed divertors, long divertor legs and ELM mitigation techniques can effectively exhaust the ELM energy before it reaches the divertor targets.

5. Scrape-Off Layer & Divertor

Finding a solution to the exhaust of heat and particles is of paramount importance for the operation of ITER and design of future reactors. The high concentration of heat and particle loads to plasma-facing surfaces in the divertor is strongly governed by a combination of filamentary transport across the scrape-off layer (SOL) and transport along the magnetic field; the resulting highly concentrated parallel heat fluxes must be reduced to avoid damaging divertor surfaces. Data from MAST experiments, together with detailed modelling, have yielded key insights into the nature of filamentary transport with a conventional open divertor in preparation for studies in alternative divertors such as the Super-X in MAST Upgrade.

The separation of filaments in the Scrape-Off Layer, the possible interactions between pairs of filaments and possible implications on the formation of radial profiles have been studied in detail through analysis of fast imaging data and numerical simulations respectively. Measurements of the toroidal separation of the filaments from camera images indicate they have a double exponential distribution [48], with the peak at ~5cm spatial separation, suggesting the lack of a toroidal mode structure. The interaction between pairs of filaments of varying size and separation has been studied with 2D and 3D simulations [49] with the BOUT++ code [50] utilising the STORM transport model [51] [52] [53]. This interaction occurs when the dipolar electrostatic fields associated with the filaments merge or cancel each other, thereby altering the centre-of-mass velocity of the pair of filaments. The interaction quickly decays with increasing filament separation, resulting in changes in their velocity of $\leq$50% for filaments seeded ~1 width apart. Conversely, filaments separated by more than 5 times their width are found to behave independently. This suggests that the impact of interactions between filaments on MAST, that are typically separated by ~5 filament widths, is expected to be modest. This finding adds credence to stochastic models that treat the SOL density profile as the superposition of non-interacting filaments. One such model [54], that treats the production of filaments as a Poisson process and includes radial transport and draining of particles and energy along field lines. It has recently been extended to accommodate filaments launched from different toroidal locations with a finite toroidal velocity, with distribution functions of the filament amplitude, radial and toroidal extent, and toroidal separation derived from comparison with fast camera data from MAST. This extended model is in good agreement with radial profiles of the average measured D_α emission profiles from the outer mid-plane and its variance. Furthermore, it indicates that the toroidal velocity does not affect the shape of time-averaged profiles in axisymmetric systems.

Understanding transport in the divertor region is challenging in experiments due to the paucity of data and diagnostic access and in simulations due to the high magnetic shear in the vicinity of the X-point and the wide range of transport, atomic, molecular and other processes at work. Nevertheless, deeper understanding is needed in order to predict the power and particle loads to divertor surfaces. High-

speed imaging of the lower divertor in MAST indicates the presence of several regions where the characteristics of the observed filaments are qualitatively different, including the far SOL of the outer leg due to filaments generated upstream and sheared by the X-point, small (~1cm) high frequency filaments close to the separatrix of the outer leg away from the X-point and in the private flux region [55], as illustrated in Figure 6. A quiescent region that appears devoid of filaments has been recently identified in the outer divertor leg in the vicinity of the X-point [56], with a radial extent spanning from the separatrix to $\psi_n \sim 1.02$, approximately 1 e-folding length of the heat flux profile from the separatrix, containing around 60% of the heat deposited to the divertor, and has been observed over a broad range of operating conditions in L and H-mode, over a wide range of electron density and auxiliary heating power. Possible explanations for the apparent quiescence of this region include the merging of filaments in the vicinity of the X-point or the prevalence of other non-filamentary transport mechanisms.

BOUT++ simulations of turbulent transport in a simplified sheared slab geometry were carried out to identify the dominant sources of heat and particle flux spreading in a divertor leg [57]. In these simulations, the dominant cross-field transport mechanism is due to the Kelvin-Helmholtz instability, driven by radial variations in the electron temperature at the target, and by extension the electrostatic potential at the sheath edge. This leads to the production of mesoscale structures which transport heat and particles from the scrape-off layer into the private flux region, whilst the interchange mechanism predominantly acts non-linearly on existing structures, propelling them anti-parallel to the curvature vector. The angle between the divertor leg and the curvature vector strongly influences transport into the private flux region via the interchange mechanism, promoting transport in inner divertor legs where the curvature is directed toward the private flux region, and against transport in outer legs. This will motivate future modelling efforts and experiments in long-leg divertors in MAST Upgrade to understand the influence of divertor geometry on heat and particle transport. The influence of a static plasma background on filament propagation was studied in 3D BOUT++ simulations in a slab geometry, including the effects of neutrals, in plasma conditions representative of those in MAST [58] [59]. They indicate the velocity of filaments increases with increasing temperature of the plasma background. Furthermore, by comparison of several models with varying complexity in the plasma-neutral interactions included, the direct interaction between filaments and neutrals was found to have minimal impact on the filament motion.

An empirical scaling of the width of the divertor heat flux footprint mapped to the outer mid-plane, λ_q, has been derived from a database of IR imaging data of L-mode pulses [60]. Impurity transport in the scrape-off layer was studied using coherence imaging that captures the radial and vertical variation of the flows of impurity ions along magnetic field lines. Coherence imaging of C^{2+} flows [61] on the high field-side in the early phase of MAST discharges where the plasma was limited on the centre column revealed counter-streaming impurity flows when high-field side gas fuelling was applied [62]. These

flow patterns have been reproduced in EMC3-EIRENE simulations, which indicate that they are driven by enhanced pressure on field lines where the gas is ionised. Motivated by these findings, the gas fuelling system on MAST Upgrade will have gas outlets at 4 poloidal positions across the centre column and multiple outlets distributed toroidally at each poloidal position to minimise the local perturbation of plasma on field lines close to the gas outlets.

The steady-state divertor loads can be mitigated by using detachment to dissipate the plasma heat flux, however deep detachment, which can also reduce the particle flux, can lead to strong radiation at the X-point and reduced core confinement. MAST-U will have unprecedented flexibility to tailor the magnetic geometry within up-down symmetric, tightly baffled divertor chambers and excellent diagnostics to improve our understanding of detachment onset and control with a radiating zone in the leg away from the X-point in conventional and alternative divertor configurations, such as the Super-X [63] [7], X-divertor [64] [65], snowflake [66] and others. The sensitivity of detachment to external control was studied using an analytic 1D model along the magnetic field [67] including heat conduction and impurity concentration to estimate the 'detachment window' in the control parameters (upstream density, power flowing into the SOL or impurity fraction), where the 'window' is the range of that control parameter between detachment starting at the target and when it reaches the X-point. It was found that, for a given divertor configuration, the detachment window is greatest for variations in the impurity concentration, followed by P_{SOL} then upstream density. The detachment window for all parameters increases with the ratio of the total magnetic field at the X-point and the divertor target. In spherical tokamaks such as MAST Upgrade where the magnetic field drops significantly across the radial extent of the divertor (as the magnetic field across the divertor varies roughly as $B \propto 1/R$), this ratio can be higher than in a typical divertor in a conventional aspect ratio device (around 3 and 1.3 respectively). If the leg is moved to large major radius, the model predicts a wider detachment window and improved real-time control of the location of the detachment front. The impact of increasing the major radius of the divertor leg was studied using SOLPS-ITER simulations in a minimally complex slot divertor geometry [68], finding that electron density increases and temperature decreases with increasing target major radius, according $f_R^2 = B_u^2/B_t^2$, the total magnetic field upstream and at the divertor target respectively, in good agreement with the modified two-point model [69] [67]. The roll-over of the divertor particle flux with increasing density, emblematic of the onset of detachment, is found to occur when T_e at the divertor target reaches ~0.6eV, independent of the strike point major radius, but the upstream density required to reach this threshold halves when f_R is doubled, suggesting the Super-X should reach detachment at much lower upstream density compared with a conventional configuration. These findings were confirmed in simulations in a realistic MAST-U geometry [70] where the upstream density is increased, shown in Figure 7, in divertor configurations where the strike point major radius in the Super-X is nearly twice that of the conventional (0.8m and 1.5m respectively). This leads to a factor 2.4 reduction in the upstream density required to reach detachment for otherwise

similar operating parameters. In simulations of the Super-X configuration where nitrogen impurity seeding into the divertor is used to reach detachment, the region of greatest radiation emission moves away from the target but its movement slows to essentially stop at the entrance to the baffled divertor at the highest seeding rates, thereby avoiding possible core confinement degradation associated with strong radiation at the X-point. In these SOLPS-ITER simulations, collisions between plasma ions and molecules is identified as an important sink of momentum at and beyond the detachment threshold. Deeper insights into the fundamental processes governing the onset and evolution of detachment have been provided by 1D simulations carried out using the BOUT++ module SD1D [71]. For MAST Upgrade-like parameters, power dissipation through radiation is required for detachment to occur, and the energy required to ionise neutrals is required to vary with T_e, either through hydrogenic or impurity radiation, is needed to reduce the target particle flux. Volume recombination is not found to play a major role except in full detachment, where it accelerates the reduction in target ion current. Recent advances in accelerating the convergence of SOLPS-ITER using the parareal algorithm [72] have resulted in the execution time of simulations being reduced by up to a factor 10 in simulations of MAST and is expected to facilitate interpretive modelling of MAST Upgrade experiments.

6. Preparations for MAST Upgrade Operations

MAST Upgrade is currently transitioning to operations, following a successful construction phase (the completed interior is shown in Figure 8). The vacuum vessel and its interior components have been baked to achieve good vacuum conditions. Activities carried out in preparation for the plasma operations have concentrated on ensuring the operating space is as wide as possible and the implementation of novel diagnostics to enable detailed physics studies. The minimum density [73] and highest β [74][75][76] achievable in tokamaks can be determined by the amplitude and spectrum of 3D error fields introduced by imperfections in the manufacture and/or alignment of the poloidal field coils. A rigorous characterisation of the intrinsic error field has been carried out through high-precision 3D measurements of the magnetic field produced by the poloidal field coils in the main chamber and divertors that indicate the dominant harmonics have toroidal mode numbers n = 1, 2. These measurements were used to determine the optimum orientation of each coil to minimise the n = 1 harmonic, which as then applied during the final alignment of the coils to an accuracy of 0.3mm. Such an error would result in a resonant m/n = 2/1 error field of amplitude normalised to the toroidal field of $\sim 1 \times 10^{-6}$ at the q=2 surface per coil in a typical equilibrium. This is expected to result in a density threshold for locked mode onset of $\sim 3 \times 10^{18}$ m^{-3} (2% of the Greenwald density limit [77] at 1MA plasma current). Active compensation of the residual n = 1 and n = 2 error fields will be carried out using a combination of ex-vessel and in-vessel coils respectively, guided by modelling using the ERGOS

vacuum model and MARS-F linear single fluid MHD code to optimise the active control of the n = 2 harmonic.

The first experimental campaign is expected to commence in 2019, utilising the new capabilities provided by the upgrade and high-resolution diagnostics to address key physics issues for the operation of ITER and the design of DEMO, principally plasma exhaust, energetic particle physics and the development of integrated scenarios. New divertor diagnostics have been installed including novel electrical modules utilising field programmable gate arrays will operate the real-time protection system, divertor Langmuir probes [78] and foil bolometer arrays [79] that will provide unprecedented flexibility and data quality. A divertor Thomson scattering system will provide spatially resolved electron temperature and density measurements across the lower divertor chamber [80].

New and improved fast particle diagnostics include an upgraded neutron camera is expected to have a time resolution of 1ms, a statistical uncertainty of less than 10% for all MAST Upgrade scenarios and a spatial resolution of 10 cm for a fixed neutron camera position. The resolution can be increased by scanning the camera lines of sight between repeated discharges. Moreover, a new scintillator-based fast ion loss detector [34] and solid-state Neutral Particle Analyser (NPA) will be installed.

Analysis of data from line-of-sight integral measurements and comparison with modelling will be significantly improved using the new CHERAB and Raysect tools [81] [82] that employ highly efficient ray tracing techniques and realistic 3D models of the machine interior to accurately simulate reflections. Synthetic representations of the primary divertor diagnostics have been developed to aid data interpretation and analysis, for example, simulated images of emission from C^{2+} ions in the lower divertor are shown in Figure 9 for a detached outer divertor. As the divertor approaches detachment, an emission front moves from the outer strike point toward the X-point and is under investigation as a means of controlling the degree of detachment in real-time.

A phased programme of enhancements is underway to address key gaps in the EUROfusion plasma exhaust strategy for finding a solution to the heat exhaust in a reactor, involving 5MW of additional NBI heating (bringing the total NBI heating power to 10MW), a cryoplant to serve the existing cryopumps, a high frequency pellet injector and new and upgraded diagnostics including new fast imaging cameras viewing the main chamber SOL and IR cameras, infrared video bolometers and a Thomson scattering system viewing the X-point [83].

7. Summary

Recent results from MAST have advanced our understanding in key areas concerning the design and operation of future fusion devices, including core transport and confinement, fast particle physics, edge transport and stability and transport and dissipation in the Scrape-Off Layer (SOL) and divertor. There

is a strong emphasis on challenging theory and models with high-resolution measurements to improve our capability to extrapolate these results to future devices.

Studies of core transport have concentrated on understanding the effects of flows on measured and simulated ion scale turbulence and understanding improved energy confinement in spherical tokamaks with decreasing collisionality. Near the non-linear stability threshold, flow shear breaks the symmetry in up-down symmetric plasmas, leading to tilted density fluctuation correlation functions and skewed fluctuation distribution functions. Electron scale turbulence in MAST has been modelled using GS2, run for sufficiently long (~1% of τ_E) for slowly growing zonal modes to break up radially elongated streamers and increase the energy confinement with decreasing collisionality, as observed in experiments.

Fast particle physics studies have concentrated on understanding the effects of sawteeth on fast ion confinement, improving predictions of fusion products and the impact of Resonant Magnetic Perturbations (RMPs) on fast particle confinement. Measurements of the fast particle population in the presence of sawteeth were compared with TRANSP/NUBEAM simulations, finding that both passing and trapped particles are redistributed in equal measure, suggesting that resonances between the m=1 perturbation and the fast ion orbits may be playing a dominant role in the fast ion transport. Measured fusion products from D-D interactions with a neutron camera and a charged fusion product detector are 40% lower than predictions from TRANSP/NUBEAM, highlighting possible deficiencies in the guiding centre approximation.

Transport at the edge of the plasma has been studied in detail using a reciprocating probe, indicating the presence of a Geodesic Acoustic Mode 2cm inside the separatrix in an ohmic L-mode plasma. The application of RMPs can lead to a 20-30% reduction in the particle confinement time in L-mode and H-mode. Initial predictions of type-I ELM evolution and transport through a Super-X divertor configuration in MAST-U have been developed, which will be used to test the influence of the extended divertor volume on the distribution and dissipation of the energy deposited to surfaces in the divertor.

New insights into turbulent transport in the SOL and divertor have resulted from a combination of detailed measurements, heuristic modelling and simulations. Fast imaging of SOL filaments viewed from the mid-plane have been used to estimate the distribution of filament separation, which has a double exponential shape, peaked at ~5 filament widths. BOUT++ simulations of interactions between pairs of filaments find that the interaction between filaments separated by 5 times their width is negligible. This validates a key assumption in a heuristic model that describes radial profiles in the SOL as the superposition of independent filaments, which reproduces the mean and variance of radial D_α emission profiles in MAST. Fast imaging of filaments viewed from the lower divertor indicate the presence of an apparently quiescent region near the X-point devoid of filaments.

The effect of varying the major radius of the divertor strike point on the onset and evolution of detachment has been modelled in preparation for experiments studying the Super-X configuration on MAST Upgrade. The sensitivity of detachment to external control has been studied using a thermal front model, predicting that operation with detached divertors should be possible over a wider region of operating space as the major radius is increased. In MAST-like conditions, BOUT++ simulations indicate that divertor particle flux mitigation necessitates power dissipation through radiation and the energy required to ionise neutrals should increase with T_e.

The construction of MAST Upgrade is complete, featuring baffled divertors with a highly flexible set of poloidal field coils to allow for detailed studies of detachment physics in alternative divertor configurations. Studies of confinement of thermal and energetic particles will benefit from a combination of increased maximum toroidal field (from 0.585T to 0.92T at R=0.7m), plasma current (from 1.35MA to 2.0MA) and a combination of on and off-axis heating. Further enhancements, part-funded by EUROfusion, are underway to increase the auxiliary heating power from 5MW to 10MW, a cryoplant to serve the existing cryopumps, a high frequency pellet injector and new and upgraded diagnostics.

Acknowledgements

This work has been carried out within the framework of the EUROfusion Consortium and has received funding from the Euratom research and training programme 2014-2018 under grant agreement No 633053 and from the RCUK Energy Programme [grant number EP/P012450/1]. To obtain further information on the data and models underlying this paper please contact PublicationsManager@ccfe.ac.uk. The views and opinions expressed herein do not necessarily reflect those of the European Commission. This work supported in part by the US Department of Energy contracts: DE-AC05-00OR22725 and DE-SC0012315.

References

[1] A. Kallenbach et al., Nucl. Fusion **57** 102015 (2017)

[2] J. E. Menard et al., Nucl. Fusion 57 102006 (2017)

[3] O. Motojima Nucl. Fusion **55** 104023 (2015)

[4] H. Zohm et al., Nucl. Fusion **53** 073019 (2013)

[5] G. Federici et al., Fusion Eng. Des. **109-111** 1464 (2016)

[6] J. Milnes et al., Fusion Eng. Des. **96-97** 42 (2015)

[7] A. W. Morris et al., IEEE Trans. Plasma Sci. **46** 5 1217-1226 (2018)

[8] M. Valovič et al., Nucl. Fusion **51** 073045 (2011)

[9] S. Kaye et al., Nucl. Fusion 47 499 (2007)

[10] C. M. Roach et al., Plasma Phys. Control. Fusion **47** B323 (2005)

[11] N. Joiner et al., Plasma Phys. Control. Fusion **48** 685 (2006)

[12] C. M. Roach et al., Plasma. Phys. Control. Fusion **48** 124020 (2009)

[13] G. J. Colyer et al., Plasma Phys. Control. Fusion **59** 055002 (2017)

[14] C. M. Roach et al., Nucl. Fusion **48** 125001 (2008)

[15] W. Guttenfelder et al., Phys. Rev. Lett. **106**, 155004 (2011)

[16] W. X. Wang et al., Nucl. Fusion **55** 122001 (2015)

[17] M. F. J. Fox et al., Plasma Phys. Control. Fusion **59** 044008 (2017)

[18] M. F. J. Fox et al., Plasma Phys. Control. Fusion **59** 034002 (2017)

[19] F. van Wyk et al., Plasma Phys. Control. Fusion **59** 114003 (2017)

[20] I. T. Chapman et al., Plasma Phys. Control. Fusion **53** 124003 (2011)

[21] M. Cecconello, A. Sperduti, Plasma Phys. Control. Fusion **60** 055008 (2018)

[22] J. Ongena, M. Evrard, D McCune, Trans. Fusion Technol. **33** 181 (1998)

[23] A. Pankin, D. McCune, R. Andre, G. Bateman, A Kritz, Commun. Comput. Phys. **159** 157 (2004)

[24] B. Kadomtsev Sov. J. Plasma Phys **1** 389 (1976)

[25] F. Porcelli et al., Plasma Phys. Control. Fusion **38** 2163 (1996)

[26] B. Madsen et al., Rev. Sci. Instrum. **89** 10D125 (2018)

[27] H. Weisen et al., Nucl. Fusion **57** 076029 (2017)

[28] M. Cecconello et al., Nucl. Instrum. Methods A **753** 72 (2014)

[29] R. V. Perez et al., Rev. Sci. Instrum. **85** 11D701 (2014)

[30] M. Cecconello et al., Nucl. Fusion "Discrepancy between estimated and measured fusion product rates on MAST using guiding-centre approximation", accepted for publication

[31] K. G. McClements et al Plasma Phys. Control. Fusion **60** 095005 (2018)

[32] A. Kirk et al., Plasma Phys. Control. Fusion **55** 124003 (2013)

[33] K. G. McClements et al Plasma Phys. Control. Fusion **60** 025013 (2018)

[34] J.F. Rivero-Rodriguez et al, Rev. Sci. Instrum. **89** 10I112 (2018)

[35] M. Jakubowski, R. J. Fonck, G. R. McKee Phys. Rev. Lett. **89** 265003 (2002)

[36] G. D. Conway et al., Plasma Phys. Control. Fusion **50** 055009 (2008)

[37] K. J. Zhao et al., Phys. Rev. Lett. **96** 255004 (2006)

[38] B. Hnat et al Plasma Phys. Control. Fusion **60** 085016 (2018)

[39] J. Adámek et al., Czech. J. Phys. **55** 235 (2005)

[40] N. R. Walkden et al., Rev. Sci. Instrum. **86** 023510 (2015)

[41] S. Murphy-Sugrue et al., Plasma Phys. Control. Fusion **59** 055007 (2017)

[42] A. Kirk et al., Nucl. Fusion **50** 034008 (2010)

[43] T. Evans et al., Phys. Rev. Lett. **92** 235003 (2004)

[44] Y. Liang et al., Phys. Rev. Lett. **98** 265004 (2007)

[45] G. P. Maddison et al., Plasma Phys. Control. Fusion **48** 71 (2006)

[46] K. Flesch et al., "Effect of RMP application on neutral fueling and exhaust in MAST", Plasma-Surface Interactions in Controlled Fusion Devices conference (2018)

[47] G.T.A. Huysmans, O. Czarny, Nucl. Fusion **47** 659 (2007)

[48] T. Farley et al., Proc 45th EPS Conf. 2018

[49] F. Militello et al., Plasma Phys. Control. Fusion 59 125013 (2017)

[50] B. D. Dudson, M. V. Umansky, X. Q. Xu, P. B. Snyder, H. R. Wilson, Comput. Phys. Commun. **180** 1467 (2009)

[51] L. Easy et al., Phys. Plasmas **21** 122515 (2014)

[52] L. Easy et al., Phys. Plasmas **23** 012512 (2016)

[53] N. R. Walkden, L. Easy, F. Militello, J. T. Omotani, Plasma Phys. Control. Fusion **58** 115010 (2016)

[54] F. Militello et al., Phys. Plasmas 25 056112 (2018)

[55] J. R. Harrison et al., Phys. Plasmas 22 092508 (2015)

[56] N. R. Walkden et al., Nucl. Fusion 57 126028 (2017)

[57] N.R.Walkden et al, subm NME, "3D simulations of turbulent mixing in a simplified slab-divertor geometry"

[58] D. Schworer et al., Nucl. Mat. Energy **12** 825 (2017)

[59] D. Schworer et al., Plasma Phys. Control. Fusion in press (2018)

[60] S. Elmore et al., Proc 45th EPS Conf. 2018

[61] S. A. Silburn et al., Rev. Sci. Instrum. **85** 11D703 (2014)

[62] I. Waters et al., Nucl. Fusion 58 066002 (2018)

[63] P. M. Valanju, M. Kotschenreuther, S. M. Mahajan, J Canik Phys. Plasmas **16** 056110 (2009)

[64] H. Takase, J. Phys. Soc. Japan 70 609 (2001)

[65] M. Kotschenreuther, P. M. Valanju, S. M. Mahajan, J. C. Wiley, Phys. Plasmas 14 072502 (2007)

[66] D. D. Ryutov Phys. Plasmas **14** 064502 (2007)

[67] B. Lipschultz, F. I. Parra, I. H. Hutchinson, Nucl. Fusion 56 056007 (2016)

[68] D. Moulton et al., Plasma Phys. Control. Fusion 59 065011 (2017)

[69] T. W. Petrie Nucl. Fusion **53** 113024 (2013)

[70] D. Moulton et al,. Proc 44th EPS Conf. 2017

[71] B. D. Dudson et al., subm. NME "The role of particle, energy and momentum losses in 1D simulations of detachment" (2018)

[72] D. Samaddar et al., Comput. Phys. Commun. **221** 19 (2017)

[73] D.F. Howell, T.C. Hender, G. Cunningham, Nucl. Fusion **47** 1336 (2007)

[74] J-K Park et al., Nucl. Fusion **52** 023004 (2012)

[75] A.M. Garofalo, R.J. La Haye, J.T. Scoville, Nucl. Fusion **42** 1335 (2002)

[76] S.A. Sabbagh et al., Nucl. Fusion **46** 635 (2006)

[77] M. Greenwald Plasma Phys. Control. Fusion **44** R27 2002

[78] J. Lovell et al., JINST 12 C11008 (2017)

[79] J. Lovell et al., Rev. Sci. Instrum. 87 11E721 (2016)

[80] J. Hawke et al JINST **8** C11010 (2013)

[81] M. Carr et al., Proc 44th EPS Conf. 2017

[82] M. Carr et al., Rev. Sci. Instrum., in press "Description of complex viewing geometries of fusion tomography diagnostics by ray-tracing" (2018)

[83] J. R. Harrison et al., Proc 43rd EPS Conf. 2016

Figures

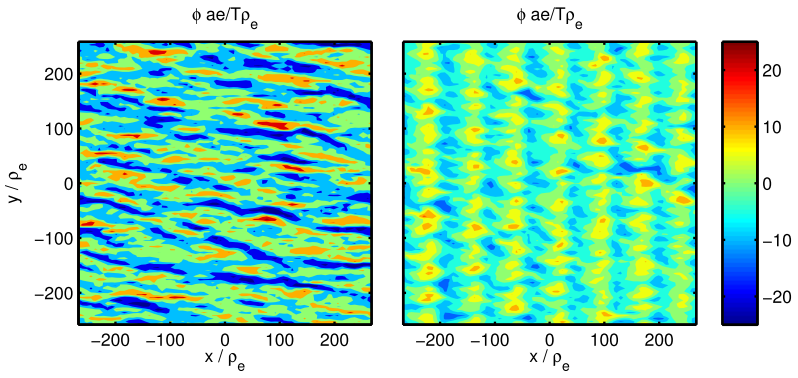

Figure 1: Normalised electrostatic potential fluctuations $e\phi/T\rho_*$ (where ρ_* is the electron Larmor radius normalised to the minor radius) at the outer mid-plane during the early quasi-saturated phase (left) and long-term saturated state (right). The collisionality is 20% of the typical values obtained in MAST experiments.

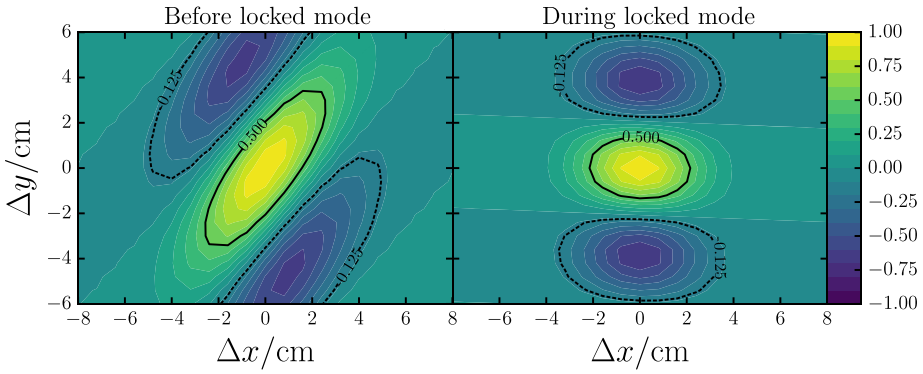

Figure 2: Spatial two-point correlation function of density fluctuations before (left) and during (right) the onset of a locked mode that reduces the toroidal flow shear.

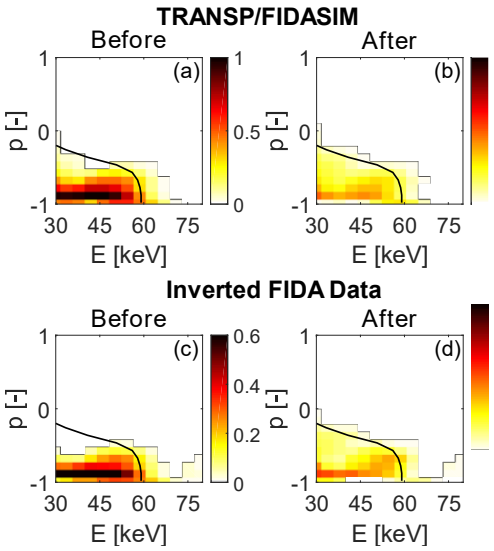

Figure 3: Reconstructions of the FIDASIM (a-b) and experimental (c-d) normalised fast ion distributions in pitch and energy before and after a sawtooth crash. The black curves mark a boundary outside which fast ions had only a low probability of being present, according to a neoclassical TRANSP simulation [26].

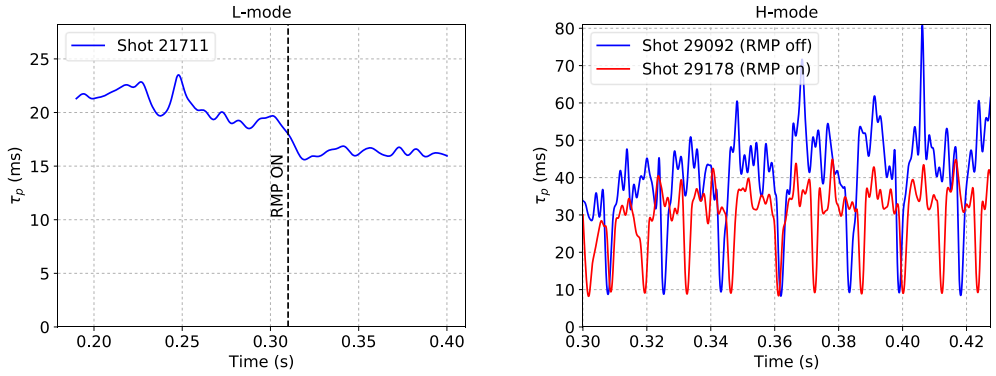

Figure 4: The impact of Resonant Magnetic Perturbations (RMPs) on global particle confinement in an L-mode (left) and H-mode plasma (right).

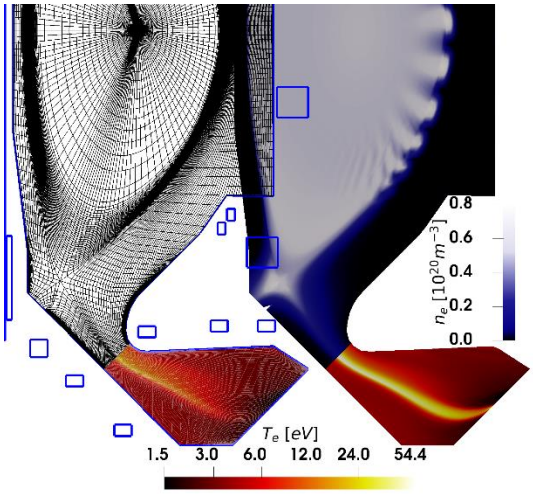

Figure 5: Predicted temperature (red) and density (blue) profiles across the MAST-U divertor chamber before (left) and after (right) the triggering of an ELM releasing a heat pulse into the divertor, simulated using JOREK.

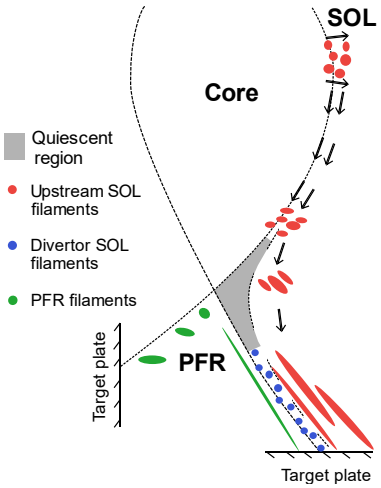

Figure 6: Schematic of the different contributions to intermittent cross-field transport in the divertor observed in MAST.

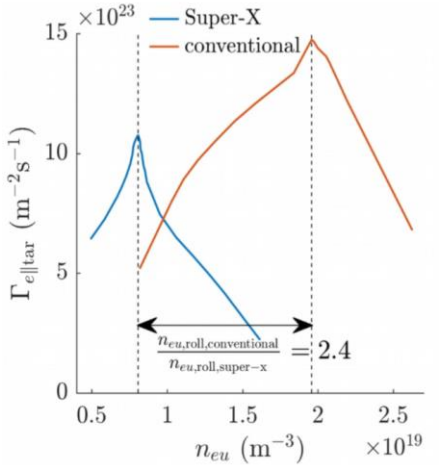

Figure 7: Roll over of the divertor target particle flux with upstream density in conventional and Super-X configurations.

Figure 8: Photograph of the completed interior of MAST Upgrade prior to being pumped down.

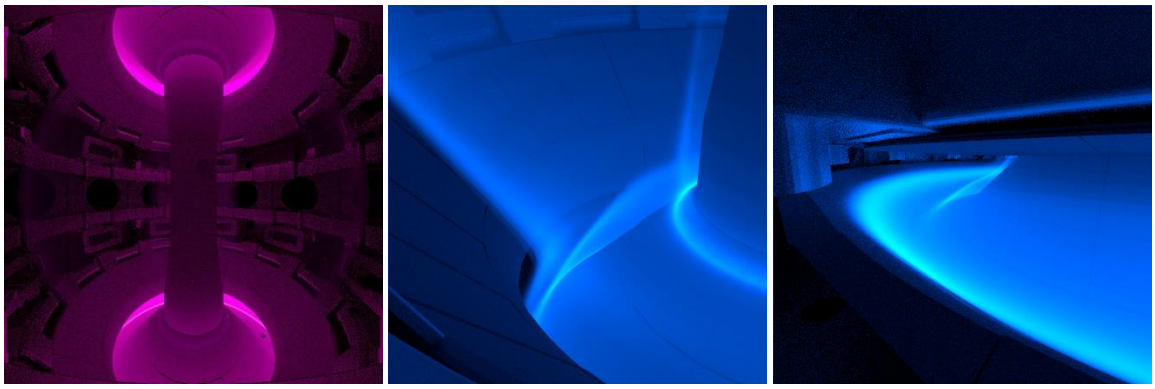

Figure 9: Synthetic camera images of emission from neutral deuterium (left) and C^{2+} ions calculated from a SOLPS simulation of MAST Upgrade as viewed from filtered cameras installed to monitor the lower X-point and inner divertor (middle) and lower divertor chamber (right).